Three Novel Sets of $Cs_2H[PW_4Mo_8O_{40}]$ Based on Various Supports: Insight into Comparative Evaluation in Oxidative Desulfurization

Akbari, Azam*[+]

Chemistry and Chemical Engineering Research Center of Iran, P.O. Box 14335-186, Tehran, I.R. IRAN

Fakhri, Hanieh

Department of Chemistry, Tarbiat Modares University, P.O. Box 14155-4383, Tehran, I.R. IRAN

ABSTRACT: *Three novel heterogeneous catalysts were prepared by immobilization of a synthesized cesium salt of 4-tungsto-8-molybdophosphoric acid (abbreviated as CW_4Mo_8) on well prepared and modified support materials of UiO-66, microsphere SBA-15 and Graphene Oxide (GO). The aim of this work was the investigation of the support effects on the Oxidative DeSulfurization (ODS) performance under a similar condition. These catalysts were characterized using FTIR, XRD, BET, BJH, N_2 adsorption-desorption, SEM, and EDX methods. The Cs modification was performed to have an insoluble CW_4Mo_8 on the support materials. The Keggin structure of the synthesized CW_4Mo_8 and well immobilization on the supports were confirmed by the characterization results. A comparative examination was performed on the capability of these nanocomposites as catalyst-adsorbent in ODS process. Dibenzothiophene (DBT) in n-hexane was used as an oil model. The examination results indicated the special impact of the support type on the catalyst design; High surface area and porosity, and functional group type significantly affected the efficiency of DBT oxidation and adsorption of $DBTO_2$ from fuel by these catalysts. The maximum removal of 100 and 99% of DBT was achieved using CW_4Mo_8 supported on mesoporous SBA-15 (after 60 min) and UiO-66 (after 120 min) respectively. Furthermore, the best catalyst could be reused four times without a remarkable decrease in activity.*

KEYWORDS: *Oxidative desulfurization; Heteropoly acids; Dibenzothiophene; UiO-66; SBA-15; Graphene oxide; Porous materials.*

INTRODUCTION

The harmful effects of sulfur compounds during fuels combustion can be along with the production of acid rain, equipment destruction and catalyst poisoning in vehicle exhaust systems. This led to create stricter environmental laws so that in US and Europe the sulfur value in diesel fuel should be less than 10 ppmw [1]. Currently,

* *To whom correspondence should be addressed.*
+ E-mail: *a.akbari@ccerci.ac.ir*
1021-9986/2020/6/149-161 *13/$/6.03*

hydrodesulfurization (HDS) as a commercial method, has been broadly employed for elimination of sulfur compounds such as sulfides, disulfides and thiols [2]. Nevertheless, this process cannot be effective for deep elimination of refractory sulfur compounds like dibenzothiophene (DBT) and its derivatives because of severe operational conditions such as high temperature and high pressure of expensive H_2 [3-6]. Considering these drawbacks, researches about finding more suitable alternatives or complementary methods had a great importance over the past few years. Under this situation, other alternative desulfurization strategies, e.g. extraction [7,8], adsorption [9,10], biodesulfurization [11,12], and photocatalytic desulfurization [13,14] have been extensively investigated. Newly, the oxidative desulfurization (ODS) is introduced as a promising alternative that has some benefits like mild reaction conditions (at temperature less than 100°C and atmospheric pressure), high selectivity and ecofriendly [15]. By this process, refractory sulfur matters are easily oxidized to polar products which can be quickly separated from oil phase by absorption or extraction [16-18]. Various catalytic systems such as layered double hydroxides, [19,20] zeolites, [21,22] ionic liquids, [23-26] organic acids [27,28] and supported solid catalysts, [17,29] are assayed for ODS reactions. Nevertheless, there are attractive reports about heteropoly acids (HPAs) compounds [30-33]. HPAs are a large group of nanosized metal-oxygen cluster anions which can be a special choice for ODS reactions due to unique acidic properties, fast reversible multi electron redox transformation, wide ranges of their acid and redox behavior, and a good stability [34]. However, there are some challenges to gain deep desulfurization by HPAs; A low surface area and high solubility in a polar solution (resulted in a hard separation and recovery) limited widely application of HPAs [35]. To address these issues, many researches focused on the use of "supported HPAs" catalysts for ODS process such as carbon [36], metal oxide [37], polyvinylalcohol [38], silica [39-41], metal organic frameworks [42-44].

In this regard, despite the type and catalytic ability of HPA, the textural properties of the support material could also be very important to have an effective ODS process. Moreover, the modification of the support may also improve the immobilization of HPAs on the support surface [45-47]. Silica, metal organic framework and graphene oxide materials are three sets of favorable supports which have been widely used in catalytic reactions. However, to select the best support for HPAs immobilization, the comparative performance of these carriers at a similar reaction conditions were not investigated in previous ODS researches. In this work, three support materials of UiO-66 metal organic framework, SBA-15 and Graphene Oxide (GO) were prepared and then modified, for the first time, by a Cesium (Cs) salt. After that, a prepared Keggin HPA of tungsten and molybdenum addenda atoms ($H_3PW_4Mo_8O_{40}$) was immobilized on the modified supports and were-used as a catalyst-adsorbent in the ODS system. The Cs modification of the supports was performed to form an insoluble salt of $Cs_2H[PMo_8W_4O_{40}].nH_2O$ on the surface for less leaching of HPAs. Furthermore, by changing of H^+ with Cs^+ cations, the Lewis acidity was enhanced that could have a promoter role in ODS process [46,47]. A high surface area, easy functionalization and good stability of these supports could be suitable factors for ODS process [45]. These synthesized nanocomposites were characterized and then tested in ODS of DBT while the effect of support type was considered for the first time. The reusability of the most effective catalyst was also investigated.

EXPERIMENTAL SECTION

Materials

All of the following used chemicals for synthesis of HPA, support materials and catalysts, as well as DBT, n-hexane and hexadecane as internal standard for ODS tests, were utilized without further purification and purchased from Merck and Sigma-Aldrich companies.

Synthesis of $H_3P\ W_4Mo_8O_{40}$

The synthesis of $H_3P\ W_4Mo_8O_{40}$ was carried out using a modified procedure reported by *Huixiong et al.* [48]. The atomic ratios of P/Mo/W were determined by ICP analysis and obtained as: 1.00/7.81/3.68. This product was labeled as W_4Mo_8.

Synthesis of Supports

Synthesis of UiO-66

At first, 0.38g $ZrCl_4$ and 0.27g 2-aminoterephthalic acid (NH_2BDC) were mixed with 20 mL dimethylformamide (DMF) and stirred for 40 min. Then, this mixture was transferred to an autoclave and heated

at 120 °C for 24 h [49]. The achieved precipitate was separated by centrifugation and washed for several times with DMF and methanol. Finally, it was dried at 120˚C.

Synthesis of microsphere SBA-15

In this procedure, 3 g of P123 ((poly (ethylene oxide)-poly (propylene oxide)-poly (ethyleneoxide)) was dissolved in 60ml HCl (2M) and stirred for 2h. Then 30 mL of dionized water was added. In the next step, 0.5 g CTAB (cetyl trimethyl amonium bromid) was dissolved in methanol and added and finally, 4 ml of TEOS (tetraethyl orthosilicate) was dropped to the prepared solution. This final mixture was refluxed for 24 h and subsequently was transferred to an autoclave and maintained at 100 °C for 18 h. The obtained sample was washed with ethanol and water. Finally, the powder was calcined at 600 °C for 6 h [50].

Synthesis of GO

The GO nanolayers were prepared by modified Hummers method [51].

Synthesis of Heterogeneous Supported Catalysts

A two-step method was used as follows: In the first step, the modification of each synthesized support (UiO-66, microsphere SBA-15 and GO) was done by aqueous incipient wetness impregnation of Cs_2CO_3 (30 wt.% Cs on the support). The collected solid was dried at 110 °C for 24 h and then calcined at 300˚C for 2 h [47]. In the second step, the impregnation of the synthesized W_4Mo_8 on the obtained Cs modified supports was done. For example, microsphere SBA-15 (0.7 g) along with W_4Mo_8 (0.3 g) and distilled water (10 mL) was stirred at 90˚C for 12 h. The obtained powder was dried at 110˚C and then calcined at 300 ˚C for 3 h. This product was labeled as CW_4Mo_8@SBA-15. A similar procedure was employed for preparation of the supported Cesium salt of W_4Mo_8 on UiO-66 (CW_4Mo_8@UiO-66) and GO (CW_4Mo_8@GO).

Characterization

The XRD patterns of as-synthesized samples were recorded on Philips X-pert diffractometer using the radiation source of Cu Kα (wavelength, λ= 1.5418 ˚A). Scanning electron microscopy (Philips XL-300 instrument) was used to assay morphology of products. Shimadzu-8400S spectrometer was employed to gain the FT-IR spectra of the synthesized samples. N_2 adsorption-desorption isotherms were obtained on a Nova Station A instrument at 77 K. The Brunauer–Emmet–Teller (BET) and the Barrett–Joyner–Halenda (BJH) methods were used for determination of the specific surface area and the pore-size distribution respectively. The sulfur compounds before and after reaction were determined by GC–MS (Agilent 7890/5975 C-GC/MSD; HP-5 MS column, 30 m ×250 μm i.d. ×0.25 μm; temperature program: 100 °C-temperature increasing 15 °C min^{-1} to 200 °C for10 min).

Catalytic Experiment

The model oil was prepared by dissolution of 2.9 g DBT in 1L n-hexane. The ODS process was performed in a 50 mL glass batch reactor as follow: 0.1g of catalyst was mixed with 25 ml of model diesel (containing 500 ppmw sulfur), 0.18 mL of 70 wt % TBHP (tert-Butyl hydroperoxide) and 0.6 mL of n-dodecane as internal standard. The mixture was stirred in a constant speed of 1000 rpm at 60˚C under reflux. The model oil samples were separated at desired times for sulfur content measurement by GC-MS.

Desulfurization efficiency was calculated by the following equation:

$$\text{Sulfur removal (\%)} = \frac{\text{Initial sulfur content} - \text{Residual sulfur content}}{\text{Initial sulfur content}}$$

RESULT AND DISCUSSION

Characterization of Catalysts

FT-IR spectra of the prepared samples were illustrated in Fig. 1. In the spectra belong to W_4Mo_8 (Fig. 1a), the characteristic peaks of kegging structure could be detected at 1051 (ν P-Oa), 951(ν M=Ot), 877 (ν M-Oc-M) and 741 cm^{-1} (ν M-Oe-M) [48]. The observed vibrational bands at 1050 and 780 cm^{-1} in Fig. 1b, were referred respectively to the stretching vibrations of Si-O-Si (asym) and Si-O-Si (sym) in the silica framework [52]. In the UiO-66 spectra (Fig. 1d), the characteristic band at 430-700 cm^{-1} was assigned to the combination of Zr–O modes with OH and CH bending vibration [53]. Furthermore, the stretching vibrations of conjugated C=C of benzene ring and C=O were located at 1612 and 1730 cm^{-1} respectively. Moreover, the N-H stretching vibration was placed at 3456 cm^{-1} in Fig. 1d. For GO sample (Fig. 1f), the spectrum contained bands at 1732, 1622, 1226 and 1056 cm^{-1}

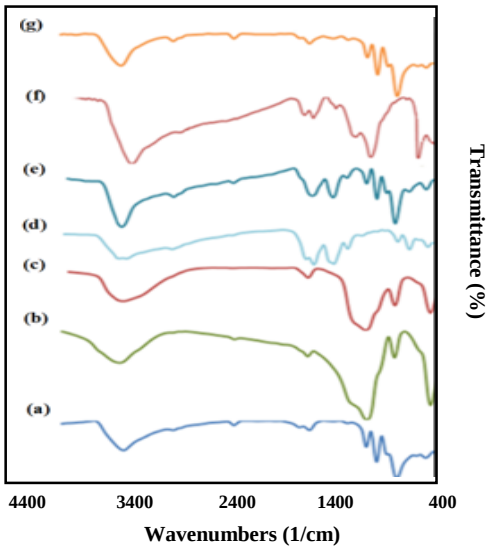

Fig.1: FT-IR spectra of W_4Mo_8(a), SBA-15(b), CW_4Mo_8@SBA-15(c), UiO-66(d), CW_4Mo_8@UiO-66(e), GO(f) and CW_4Mo_8@GO(g).

that were respectively corresponded to C=O, C=C, C-O-C and C-O stretching vibrations [54]. In the spectrum of SBA-15, the Si-O-Si symmetric and asymmetric stretching vibrations of mesoporous silica are appeared at 780 and 1050 cm^{-1}, respectively. So the characteristic bands of keggin structure of HPA are covered by frequencies of silica support. Nevertheless, in comparison with pure SBA-15, supported HPAs spectra show a slight shift that can be contributed to the interactions due to the formation of cesium salt of heteropolyacids on the surfaces of support. As seen in Fig. 1c, e and g, the FT-IR spectra of the nanocomposite indicated the main characteristic bands of both support and W_4Mo_8, although some of peaks had an overlap with together. However, a slight shift was also detectable for spectra belong to nanocomposites comparing to the pure supports that could be corresponded to the formation of a cesium salt of W_4Mo_8 on the surface of the supports [55]. This observation confirmed a successful formation of nanocomposites under the mentioned conditions.

To assay the purity and crystalline phase of as-synthesized samples, XRD patterns were illustrated in Fig. 2. The XRD pattern of W_4Mo_8 in Fig. 2a, was well matched with its Keggin structure [47]. No peak was observed in high angle XRD pattern of SBA-15 because of its amorphous feature (Fig. 2b) [56]. Fig. 2c revealed that the Keggin structure of W_4Mo_8 was well-maintained after immobilization on SBA-15. Although, the reduction in intensity and a minor shift to higher angles had been observed possibly coming from incorporation of W_4Mo_8 into mesoporous channels of silica. The XRD pattern of SBA-15 exhibited a sharp peak at $2\theta=0.58^{\circ}$ which can be indexed to (100) plane of ordered mesoporous silica channels (Fig. 2h) [55]. This characteristic peak was retained in the XRD pattern of CW_4Mo_8@SBA-15, however a decrease in its intensity was observed that can be corresponded to a change in arrangement of ordered channels belong to silica through immobilization of W_4Mo_8. For the case of UiO-66, the peaks in Fig. 2d were in agreement with previous reports that verified its formation without any impurities [57]. As shown in Fig. 2e, the major XRD pattern of UiO-66 was also detected after immobilization of W_4Mo_8; this confirmed that UiO-66 was not disturbed by W_4Mo_8 loading. In the XRD pattern of GO (Fig. 2f), the peak placed at $2\theta=11^{\circ}$ was assigned to (001) crystalline plane of GO [58]. In Fig. 2g, similar with Fig. 2c and e, the presence of W_4Mo_8 was well detectable. The crystal spacing for (100) plane of CW_4Mo_8@SBA-15 is 21.5 ˚A, for (111) plane of CW_4Mo_8@UiO- 66 is 18.51 ˚A, and for (001) plane of CW_4Mo_8@GO is 10.81˚A

N_2 absorption-desorption isotherms of the prepared samples were indicated in Fig. 3. These isotherms for SBA-15 and CW_4Mo_8@SBA-15, UiO-66 and CW_4Mo_8@UiO-66 are categorized as type IV signifying mesoporosity of them. The shape of isotherms belongs to CW_4Mo_8@GO, was attributed to types III according to IUPAC classification indicating the existence of macroporous window. The surface area and pore characteristic of all samples were represented in Table 1. As seen, the CW_4Mo_8@SBA-15 has a more surface area than other nanocomposites that can be an effective parameter in ODS reaction.

It should be noted that the GO has a low specific surface area of 65.01 $m^2.g^{-1}$ and total pore volume 0.15 cm^3/g. However, it has a flat structure that can be appropriate for immobilizing of HPAs, although its surface area is relatively low compared to SBA-15 (670.06 m^2/g) and UiO-66 (856.06 m^2/g).

To investigate morphology of the samples, SEM analysis was used. Fig. 4a indicated the microsphere of SBA-15 which was modified by Cesium and coated by W_4Mo_8 nanoparticles (Fig. 4b). The octahedral shape of UiO-66 was well observed in Fig. 4c that had a size

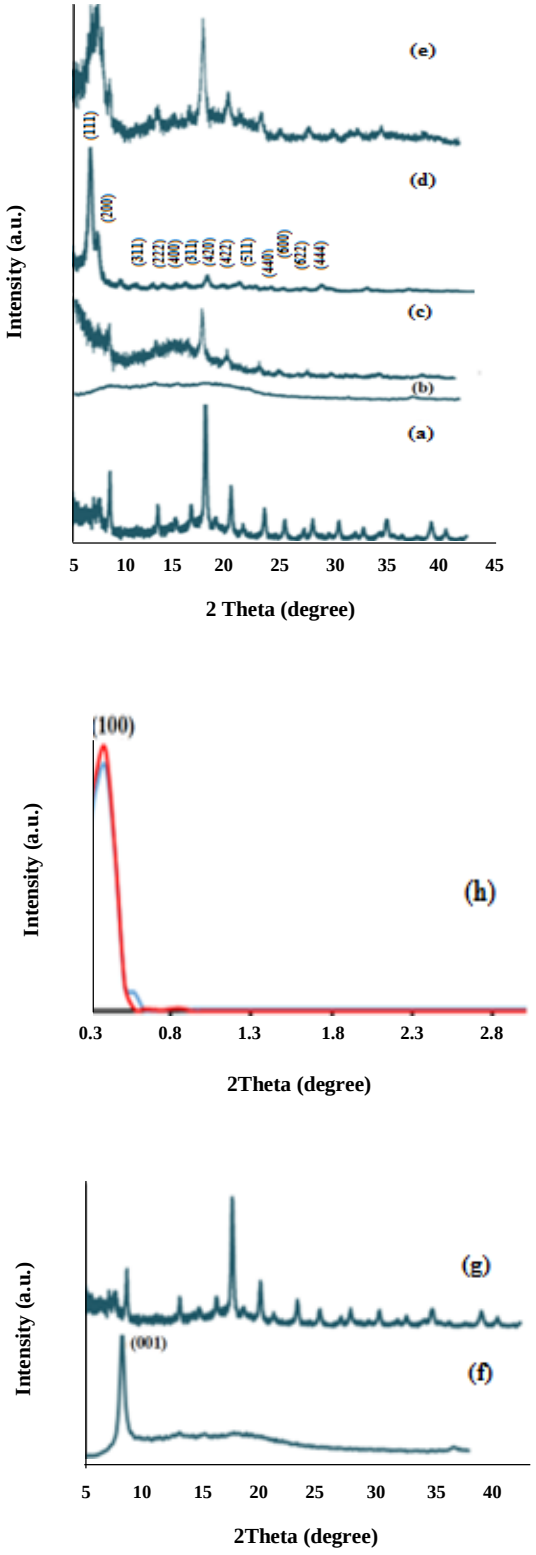

Fig. 2: High angle XRD patterns of W_4Mo_8 (a), SBA-15 (b), CW_4Mo_8@SBA-15 (c), UiO-66(d), CW_4Mo_8@UiO-66 (e), GO (f), CW_4Mo_8@GO (g) and low angle XRD pattern of SBA-15 (red pattern) and CW_4Mo_8 @SBA-15 (blue pattern) (h)

between 200-250 nm. The presence of W_4Mo_8 nanoparticles on the surface of UiO-66 was well detectable (Fig. 4d). The comparison between the images of the GO supports before and after immobilization (Fig. 4e and f), illustrated a highly dispersion of W_4Mo_8 nanoparticles on the layers of GO support.

Furthermore, the main grain size of CW_4Mo_8 in CW_4Mo_8@SBA-15 was 110 nm and as seen in fig.4d,f, high agglomeration of CW_4Mo_8 was occurred that led to a significant increase in grain size up to 540 nm. EDX analysis has been indicated in Fig. 5. It verified the presence of P, W, Mo, O, and Cs elements for all prepared samples. In the pattern belong to CW_4Mo_8@UiO-66, the presence of Zr peak belong to UiO-66 was well visible, while in CW_4Mo_8@SBA-15 and CW_4Mo_8@Go the presence of Si and C were confirmed respectively.

Comparison of Various Catalysts in ODS System

Fig. 6 indicated the comparative ODS efficiency of the prepared catalysts. These experiments were performed at 60˚C for 120 min, using 0.1 gr of catalyst and initial sulfur concentration of 500 ppmw. Fig.6 revealed that all of the catalysts had an ability for sulfur removal of model oil. However, a significant difference was observed between the performance of the catalysts immobilized on different supports. The order of CW_4Mo_8@SBA-15> CW_4Mo_8@UiO-66> CW_4Mo_8@GO was found for the performance of the catalysts in ODS of DBT. After 60 min, 100% removal of DBT was attained using CW_4Mo_8@SBA-15, while 79 and 38% of DBT elimination was obtained using CW_4Mo_8@UiO-66 and CW_4Mo_8@GO respectively. Furthermore, after 120 min, 99 and 59 % removal of DBT was achieved using CW_4Mo_8@ UiO-66 and CW_4Mo_8@ GO, respectively. To clarify the catalytic activity, it was appropriate to describe the mechanism of the reactions firstly. Based on the previous reports [59-61] and our results, the following mechanism was proposed (Fig. 7). At first, W_4Mo_8 (WM) received an oxygen from TBHP (T) and turned into peroxometalate intermediate (WM*).

$$First\ step: WM + T \rightarrow WM*$$

Consequently, this active intermediate supplied oxygen for DBT to form dibenzothiophene sulfoxide (DBTO).

$$Secound\ step: WM* + DBT \rightarrow DBTO$$

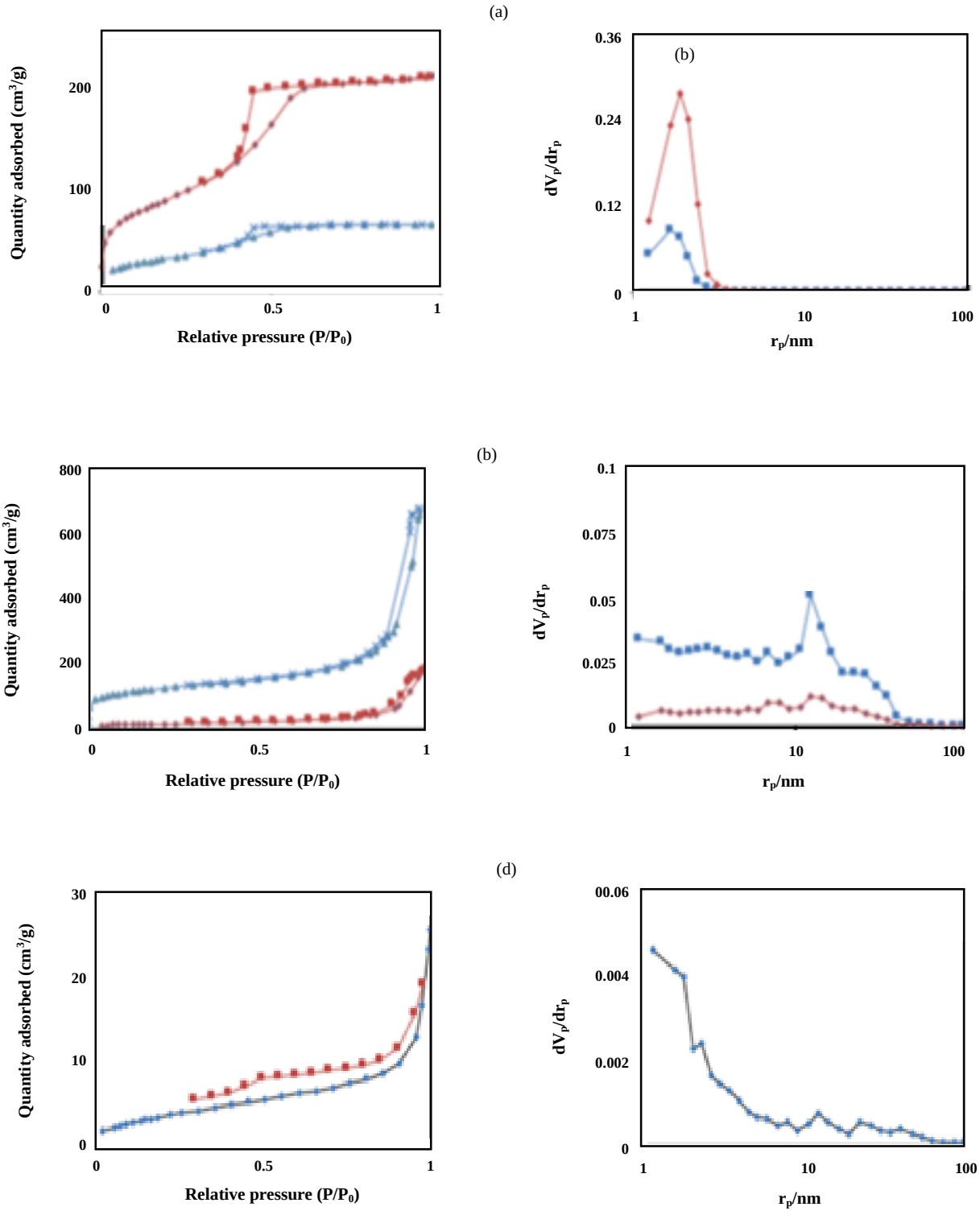

Fig. 3: N_2 adsorption–desorption isotherms and the BJH pore-size distribution of (a) CW_4Mo_8@SBA-15 (red isotherm) and SBA-15 (blue isotherm); (b) CW_4Mo_8@UiO-66(red isotherm) and UiO-66 (blue isotherm); and (c) CW_4Mo_8@GO (red isotherm) and GO (blue isotherm).

Table 1: Surface area, average pore size distribution and pore volume of samples.

Sample	BET surface(m^2/g)	Total pore volume(cm^3/g)	Mean pore diameter (nm)
CW_4Mo_8@SBA-15	330.64	0.32	3.99
CW_4Mo_8@ UiO-66	70.06	0.27	15.86
CW_4Mo_8@GO	14.11	0.03	10.26
GO	65.01	0.15	-

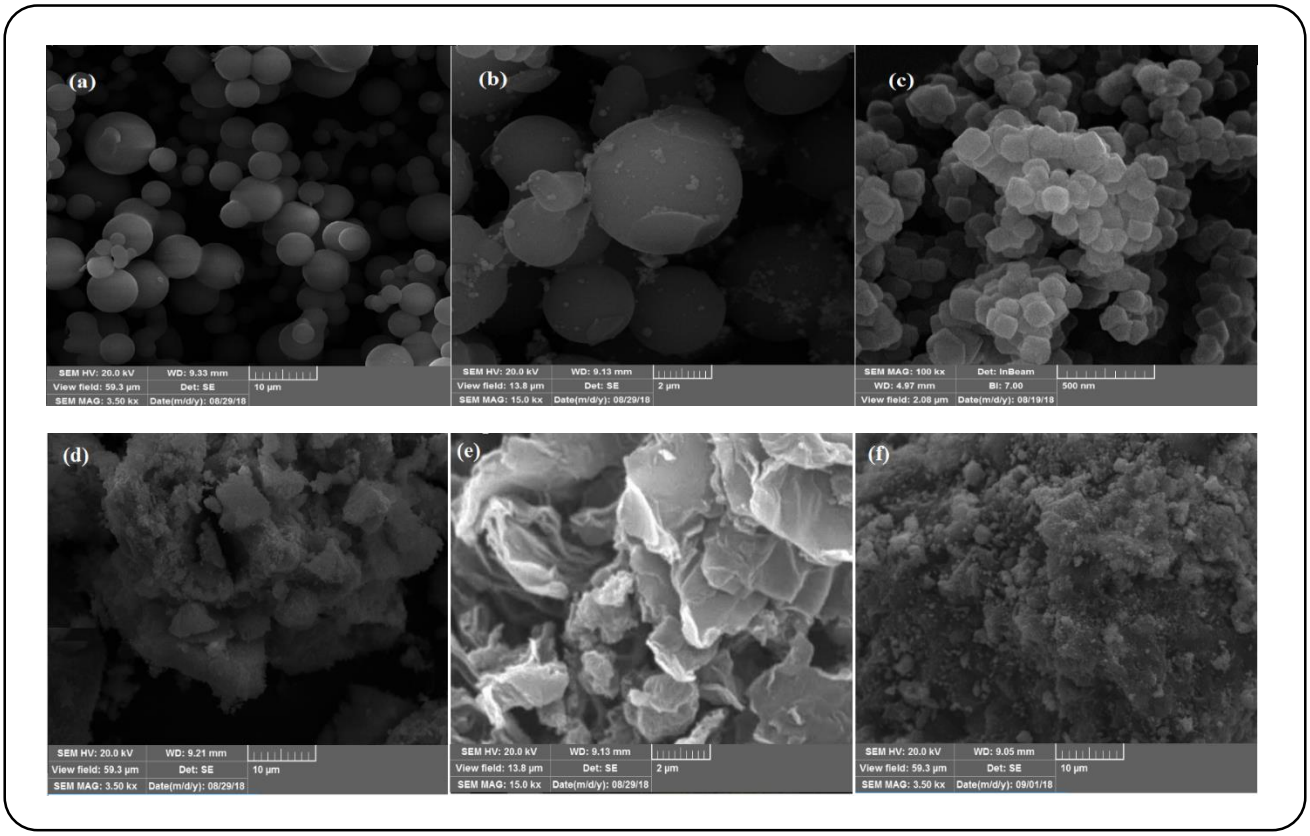

Fig. 4: SEM images of SBA-15(a), CW_4Mo_8@SBA-15(b), UiO-66(c), CW_4Mo_8@UiO-66(d), GO(e) and CW_4Mo_8@GO(f).

Another generated peroxometalate from W_4Mo_8 and TBHP, oxidized DBTO to its corresponding sulfone ($DBTO_2$) by a subsequent oxygen capturing.

$Third\ step: WM * + DBTO \rightarrow DBTO2$

According to a higher polarity of $DBTO_2$ than DBT, it could be easily adsorbed on the surface of the catalyst. In the final step, $DBTO_2$ products can be collected by separation of the solid catalyst and then washing with a polar solvent. No peak corresponded to $DBTO_2$ was observed in GC analysis of the oil after ODS which confirmed well adsorption of $DBTO_2$ by the porous supported catalysts. The main steps in this ODS pathway regarding to different supports, were the accessibility of DBT and oxidant intermediates as well as $DBTO_2$ onto the catalyst surface. Clearly, the increasing surface area provided a better access of DBT to the active oxidant intermediates generated on the surface, so a more effective ODS reaction was occurred. Besides, a higher surface area increased the adsorption capacity for $DBTO_2$ on the surface and finally resulted in an enhancement of ODS efficiency. According to Table 1, among the three catalysts, CW_4Mo_8@SBA-15 had the maximum surface area. As discussed above, the surface area of CW_4Mo_8@SBA-15 has a special effect on more accessibility of the oxidant and DBT to the active sites, and thus enhanced the ODS reactions, ultimately leading to

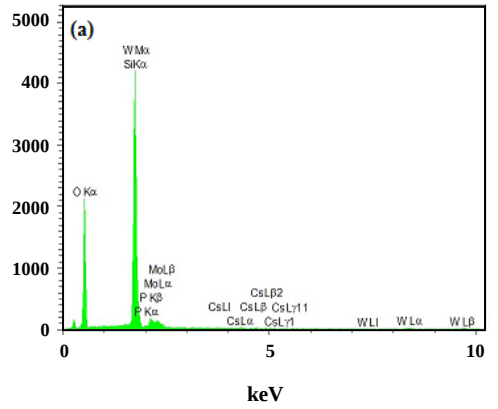

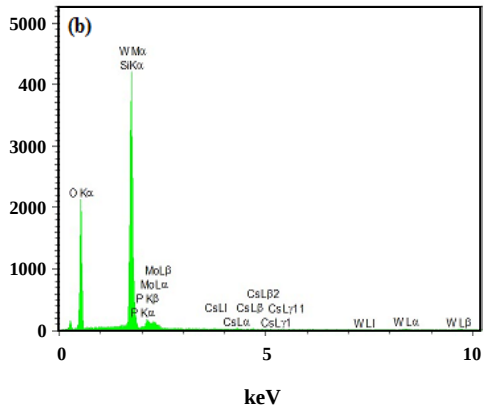

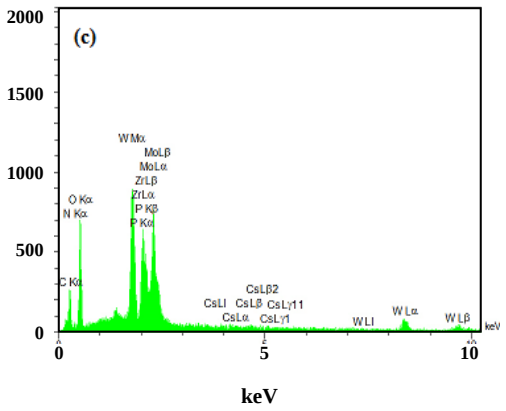

Fig. 5: EDX analysis of CW_4Mo_8@SBA-15(a), CW_4Mo_8@UiO-66(b), and CW_4Mo_8@GO(c).

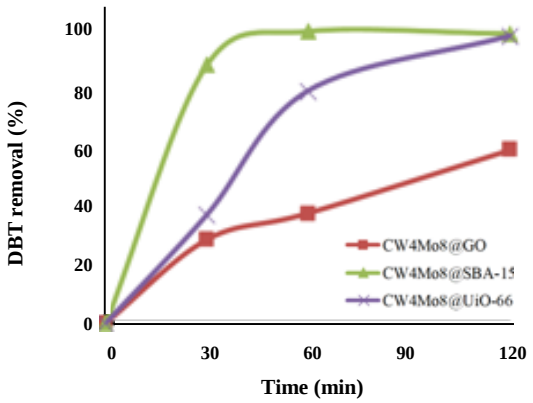

Fig. 6: Oxidative desulfurization of DBT by different modified supported catalysts

increase in efficiency. Moreover, the larger pore volume belonged to CW_4Mo_8@SBA-15 led to a less pore blockage and thus the mobility of the active peroxometalate units occurred with a faster rate compared with the other nanocomposites. For CW_4Mo_8@UiO-66, the creation of hydrogen bonding between DBT molecules with amine and carboxylic acid functional groups (from 2-aminoterephthalic acid ligand in UiO-66 framework), resulted in the increase of DBT presence around the active sites; Furthermore, the π-π interactions between the benzene ring of UiO-66 and DBT caused to more adsorption of DBT from oil on the catalyst surface for oxidation reaction. However, the smaller pore volume slightly limited ODS performance of UiO-66 comparing to SBA-15. Therefore, the functional groups had an important effect on the catalyst activity similar to the surface area and porosity. This effect had also been used for design of the proper cation and anion structure for an appropriate extractant/catalyst dual-function ionic liquid for ODS process, usually [23,24]. As seen in Fig. 4e and f, the GO layers were agglomerated in some area that could explain its lower catalytic ability in ODS process.

To evaluate the efficiency of the optimum catalyst (CW_4Mo_8@SBA-15) for industrial applications, the recovery tests were also essential. For this examination, after each ODS run, the recycled catalyst was washed by methanol for several times and dried at 110 °C for 12 h, then used in the next ODS run. The ODS efficiency decreased only 7% after 4 recycling (Fig. 8) which confirmed the stability of the catalyst and low leaching of W_4Mo_8

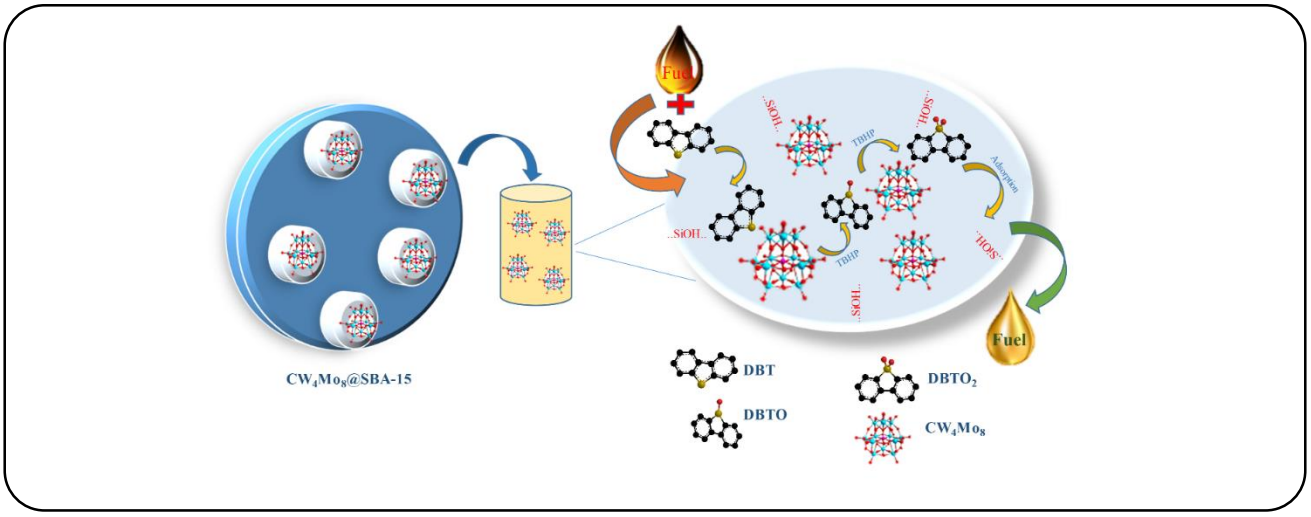

Fig. 7: The proposed mechanism of ODS in the presence of the synthesized catalysts

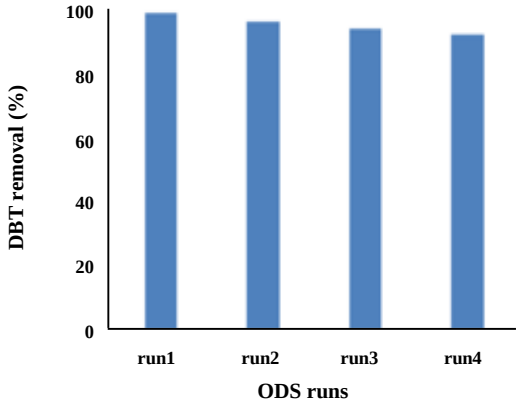

Fig. 8: Recyclability of the synthesized CW_4Mo_8@SBA-15.

(that has a main role in ODS system) by formation of an insoluble Cs salt of W_4Mo_8 on the surface.

CONCLUSIONS

In summary, three sets of cesium salt of W_4Mo_8 immobilized on Cs modified supports including SBA-15, UiO-66 and Go were prepared using the impregnation method, then were characterized by XRD, FT-IR, SEM, EDX and BET analyses. FT-IR spectra confirmed a successful formation of nanocomposites and impregnation of HPA on the support by the used approaches. Moreover, XRD results revealed that the Keggin structure of W_4Mo_8 was well-maintained after immobilization on the supports. Micro-spherical shape of modified SBA-15, octahedral shape of UiO-66 and layers of GO were observed by SEM images. Surface area of three catalysts followed the order of CW_4Mo_8@SBA-15>> CW_4Mo_8@UiO-66> CW_4Mo_8@GO, based on BET results.

The catalytic activity of the synthesized catalysts was assayed for the ODS of DBT (500 ppm). The results indicated that desulfurization efficiency strongly depends on the type of support and, all catalysts have positive effect on DBT removal, however the efficiency of CW_4Mo_8@SBA-15 was superior to other nanocomposites where 100% removal efficiency was obtained after 60 min. Its better performance was attributed to its high surface area, large pore volume, as well as a good incorporation of W_4Mo_8 into mesoporous channels of silica based on XRD results. While the smaller pore volume of UiO-66 and agglomeration of GO layers led to relatively limit the activities of CW_4Mo_8@UiO-66 and CW_4Mo_8@GO in ODS process. Despite relatively low surface area and porosity of CW_4Mo_8@UiO-66, the amine and carboxylic acid functional groups as well as the benzene rings in the structure enhanced its catalytic activity. Subsequently, the best proposed catalyst of CW_4Mo_8@SBA-15 provided a high reusability which had no significant loss of activity during 4 recycling. The leaching of CW_4Mo_8 from the support was limited through Cs modification. This work also underlined the importance of catalyst design to have a high efficient and profitable ODS system. Following the favorable results achieved in this study, other efficient nanocomposite based POM catalysts will be synthesized to enhance the catalytic desulfurization efficiency using the real diesel model.

Acknowledgment

The financial support of this study by Iran National Science Foundation (INSF) under grant No. 96011337 is gratefully acknowledged. We are also thankful to Tarbiat Modares University for technical support.

Received : Apr. 16, 2019 ; Accepted :Aug. 5, 2019

REFERENCES

[1] Faghihian H., Naeemi S., Application of a Novel Nanocomposite for Desulfurization of a Typical Organo Sulfur Compound, *Iran. J. Chem. Chem. Eng. (IJCCE)*, **32**: 9-15 (2013).

[2] Diana J., Rita V., Jorge C.R., Baltazar de C., Salete S.B., Efficient Eco-sustainable Ionic Liquid-Polyoxometalate Desulfurization Processes for Model and Real Diesel, *Appl. Catal.*, **537**: 93-99 (2017).

[3] Rothlisberger A., Prins R., Intermediates in the Hydrodesulfurization of 4,6-dimethyl-Dibenzothiophene over Pd/γ-Al_2O_3, *J. Catal.*, **235**: 229-240 (2005).

[4] Javadli R., Klerk A., Desulfurization of Heavy Oil–Oxidative Desulfurization (ODS) As Potential Upgrading Pathway for Oil Sands Derived Bitumen, *Energy Fuels*., **26**: 594-602 (2012).

[5] Tuxen A.K., Fuchtbauer H.G., Temel B., Hinnemann B., Topsoe H., Knudsen K.G., Besenbacher F., Lauritsen J.V., Atomic-Scale Insight into Adsorption of Sterically Hindered Dibenzothiophenes on MoS_2 and Co–Mo–S Hydrotreating Catalysts, *J. Catal.*, **295**: 146-154 (2012).

[6] Ma X., Sakanishi K., Mochida I., Hydrodesulfurization Reactivities of Various Sulfur Compounds in Vacuum Gas Oil, *Ind. Eng. Chem. Res.*, **35**: 2487-2494 (1996).

[7] Julião D., Gomes A,C., Pillinger M., Valença R., Ribeiro J.C., Gonçalves I.S., Balula S.S., Desulfurization of Liquid Fuels by Extraction and Sulfoxidation Using H_2O_2 and [$CpMo(CO)_3R$] as Catalysts, *Appl. Catal. B Environ.*, **230**: 177-183 (2018).

[8] Gao S., Li J., Chen X., Abdeltawab A.A., Yakout S.M., Yu G., A Combination Desulfurization Method for Diesel Fuel: Oxidation by Ionic Liquid with Extraction by Solvent, *Fuel*., **224**: 545-551 (2018).

[9] Zou C., Zhao P., Ge J., Qin Y., Luo P., Oxidation/Adsorption Desulfurization of Natural Gas by Bridged Cyclodextrins Dimer Encapsulating Polyoxometalate. *Fuel*., **104**: 635-640(2013).

[10] Zheng M., Hu H., Ye Z., Huang Q., Chen X., Adsorption Desulfurization Performance and Adsorption-Diffusion Study of B_2O_3 Modified Ag-CeO_x/TiO_2-SiO_2, *J. Hazardous Mat.*, **362**: 424-435 (2019).

[11] Yi Z., Ma X., Song J., Yang X., Tang Q., Investigations In Enhancement Biodesulfurization of Model Compounds by Ultrasound Pre-Oxidation, *Ultrason. Sonochem*., **54**: 110-120 (2019).

[12] Ye J., Zhang P., Zhang G., Wang S., Nabi M., Zhang Q., Zhang H., Biodesulfurization of High Sulfur Fat Coal with Indigenous and Exotic Microorganisms, *J. Clean Prod.*, **197**: 562-570 (2018).

[13] Ming Liang Kang, Xiang Wang, Jing Zhang, Yao Lu, Xuebing Chen, Lina Yang, Fangfang Wang, Boosting the Photocatalytic Oxidative Desulfurization of Dibenzothiophene by Decoration of MWO_4 (M=Cu, Zn, Ni) on WO_3, *J. Environ. Chem. Eng*., **7**: 102809 (2019).

[14] Xuhe L., Xiuna Y., Feng Z., Jian Z., Hao Y., Wang Y., Zhao X., Yuan X., Ju J., Hu Sh., Construction of Novel Amphiphilic $[Bmin]_3PMo_{12}O_{40}$/g-C_3N_4 Heterojunction Catalyst with Outstanding Photocatalytic Oxidative Desulfurization Performance under Visible Light, *J. Taiwan. Inst. Chem. E.*, **100**: 210-219 (2019).

[15] Mjalli F.S., Ahmed O.U., Al-Wahaibi T., Al-Wahaibi Y., AlNashef I.M., Deep Oxidative Desulfurization of Liquid Fuels, *Rev. Chem. Eng*., **30**: 337-378 (2014).

[16] Campos-Martin J.M., Capel-Sanchez M.C., Perez-Presas P., Fierro J.L.G., Oxidative Processes of Desulfurization of Liquid Fuels, *J. Chem. Technol. Biotechnol.*, **85**: 879-890 (2010).

[17] Akbari A., Omidkhah M.R., Towfighi Darian J., Facilitated and Selective Oxidation of Thiophenic Sulfur Compounds Using MoOx/Al_2O_3-H_2O_2 System under Ultrasonic Irradiation., *Ultrasound. Sonochem.*, **23**: 231-237 (2015),

[18] Akbari A., Omidkhah M.R., Towfighi Darian J., Investigation of Process Variables and Intensification Effects of Ultrasound Applied in Oxidative Desulfurization of Model Diesel over MoO_3/Al_2O_3 Catalyst, *Ultrason. Sonochem.*, **21**: 692-705 (2014).

[19] Maciuca A.L., Ciocan C.E., Dumitriu E., Fajula F., Hulea V., V-, Mo- and W-Containing Layered Double Hydroxides as Effective Catalysts for Mild Oxidation of Thioethers And Thiophenes with H_2O_2, *Catal. Today.*, **138**: 33-37 (2008).

[20] Hulea V., Maciuca A.L., Fajula F., Dumitriu E., Catalytic Oxidation of Thiophenes and Thioethers with Hydrogen Peroxide in the Presence of W-Containing Layered Double Hydroxides, *Appl. Catal. A.*, **313**: 200-207 (2006).

[21] Honarmand S., Moosavi E., Karimzadeh. Synthesis of Zeolite Y from Kaolin and Its Model Fuel Desulfurization Performance: Optimized by Box-Behnken Method, *Iran. J. Chem. Chem. Eng. (IJCCE)*, **39(1)**: 78-90 (2020).

[22] Du S., Li F., Sun Q., Wang N., Jia M., Yu J., A Green Surfactant-Assisted Synthesis of Hierarchical TS-1 Zeolites with Excellent Catalytic Properties for Oxidative Desulfurization., *Chem. Commun.*, **52**: 3368-3371 (2016).

[23] Azimzadeh H., Akbari A., Omidkhah M.R., Catalytic Oxidative Desulfurization Performance of Immobilized NMP.$FeCl_3$ Ionic Liquid on γ-Al_2O_3 Support, *Chem. Eng. J.*, **320**: 189-200 (2017).

[24] Andevary H. H., Akbari A., Omidkhah M.R., High Efficient and Selective Oxidative Desulfurization of Diesel Fuel Using Dual-Function [Omim]$FeCl_4$ as Catalyst/Extractant, *Fuel Process. Tech.*, **185**: 8-17 (2019).

[25] Nie Y., Dong Y.X., Bai L., Dong H.F., Zhang X.P., Fast Oxidative Desulfurization of Fuel Oil Using Dialkylpyridinium Tetrachloroferrates Ionic Liquids, *Fuel*., 103: 997-1002 (2013).

[26] Jiang W., Zhu W.S., Chang Y.H., Li H.M., Chao Y.H., Xiong J., Liu H., Yin Sh., Oxidation of Aromatic Sulfur Compounds Catalyzed by Organic Hexacyanoferrates in Ionic Liquids with a Low Concentration of H_2O_2 as an Oxidant, *Fuel.*, **28**: 2754-2760 (2014).

[27] Mesroghli Sh., Perman J.Y., Jorjani E., Vandewijngaarden J., Reggers G., Carleer R., Noaparast M., Changes and Removal of Different Sulfur forms after Chemical Desulfurization by Peroxyacetic Acid on Microwave Treated Coals, *Fuel*., 154: 59-70 (2015).

[28] Krivtsov E.B., Golovko A.K., The Kinetics of Oxidative Desulfurization of Diesel Fraction with a Hydrogen Peroxide-Formic Acid Mixture, *Pet. Chem.*, **54**: 51-57 (2014).

[29] Lidong W., Juan W., Peiyao X., Qiangwei L., Wendi Z., Shuai C., Selectivity of Transition Metal Catalysts in Promoting the Oxidation of Solid Sulfites in Flue Gas Desulfurization, *Appl. Catal. A.*, **508**: 52-60 (2015).

[30] Li C., Zha B., Yao Z., Jiang Z., Liquid Polyoxometalate-Based Catalysts Lead to Highly Efficient Desulfurization of Waste Water, *Polyhedron.*, **159**: 176-181 (2019).

[31] Gao Y., Lv Z., Gao R., Zhang G., Zheng Y., Zhao J., Oxidative Desulfurization Process of Model Fuel under Molecular Oxygen by Polyoxometalate Loaded in Hybrid Material CNTs@MOF-199 as Catalyst, *J. Hazard. Mater.*, **359**: 258-265 (2018).

[32] Hao X.L., Ma Y.Y., Zang H.Y., Wang Y.H., Li Y.G., and Wang E.B., A Polyoxometalate-Encapsulating Cationic Metal–Organic Framework as a Heterogeneous Catalyst for Desulfurization, *Chem. Eur. J.*, **21**: 3778-3784 (2015).

[33] Zhu W., Wu P., Chao Y., Li H., Zou F., Xun S., Zhu F., Zhao Z., A Novel Reaction-Controlled Foam-Type Polyoxometalate Catalyst for Deep Oxidative Desulfurization of Fuels, *Ind. Eng. Chem. Res.*, **52**: 17399-17406 (2013).

[34] Yu F., Liu C., Yuan B., Xie C., Yu S., Self-Assembly Heteropoly Acid Catalyzed Oxidative Desulfurization of Fuel with Oxygen, *Catal Commun*, **68**: 49-52 (2015).

[35**]** Tang L., Luo G., Zhu M., Kang L., Dai B., Preparation, Characterization and Catalytic Performance of HPW-TUD-1 Catalyst on Oxidative Desulfurization, *J. Ind. Eng. Chem.*, **19**: 620-626 (2013).

[36] Ghubayra R., Nuttall C., Hodgkiss S., Craven M., .Kozhevnikova E.F., Kozhevnikov I.V., Oxidative Desulfurization of Model Diesel Fuel Catalyzed by Carbon-Supported Heteropoly Acids, *Appl Catal B: Environ*, **253**: 309-316 (2019).

[37] Yue D., Jiaheng L., Lina Z., Zhenran G., Xiaodi D., Junsheng L., Highly Efficient Deep Desulfurization of Fuels by Meso/Macroporous $H_3PW_{12}O_{40}/TiO_2$ at Room Temperature, *Mater Res Bull.*, **105**: 210-219 (2018).

[38] Rezvani M.A., Oveisi M., Nia Asli A., Phosphotungestovanadate Immobilized on PVA as an Efficient and Reusable Nano Catalyst for Oxidative Desulphurization of Gasoline, *J Mol Catal A: Chem.*, **410**: 121-132 (2015).

[39] Yue D., Lei J., Peng Y., Li J., Du X, Hierarchical Ordered Meso/Macroporous $H_3PW_{12}O_{40}/SiO_2$ Catalysts with Superior Oxidative Desulfurization Activity, *J. Porous Mat.*, **25**: 727-734 (2018).

[40] Zhu W., Gu Q., Juan Hu J., Wu P., Yin S., Zhu F., Zhang M., Xion J., Li H., Fabrication of Functional Dual-Mesoporous Silicas by Using Peroxo-Tungstate Ionic Liquid and Their Applications in Oxidative Desulfurization, *J. Porous Mat.*, **22**: 1227-1233 (2015).

[41] Craven M., Xiao D., Kunstmann-Olsen C., Kozhevnikova E., Blanc F., Steiner A., Kozhevnikov I., Oxidative Desulfurization of Diesel Fuel Catalyzed by Polyoxometalate Immobilized on Phosphazene-Functionalized Silica, *Appl. Catal. B.*, **231**: 82-91 (2018).

[42] Yan L., Duan T., Huang T., Zhao B., Fan Y., Phosphotungstic Acid Immobilized on Mixed-Ligand-Directed UiO-66 for the Esterification of 1-Butene with Acetic Acid to Produce High-Octane Gasoline, *Fuel.*, 245: 226–232(2019).

[43] Yang X.L., Qiao L.M., Dai W.L., Phosphotungstic Acid Encapsulated in Metal-Organic Framework UiO-66: an Effective Catalyst for the Selective Oxidation of Cyclopentene to Glutaraldehyde, *Micropor Mesopor Mat.*, **211**: 73-81(2015).

[44] Zeng L., Xiao L., Long Y., Shi X., Trichloroacetic Acid-Modulated Synthesis of Polyoxometalate@UiO-66 for Selective Adsorption of Cationic Dyes, *J. Colloid Interf Sci.*, **516**: 274–283 (2018).

[45] Ribeiro S.O., Julião D., Cunha-Silva L., Domingues V.F., Valença R., Ribeiro J.C., Castro B.D., Balula S.S., Catalytic Oxidative/Extractive Desulfurization of Model and Untreated Diesel Using hybrid Based Zinc-Substituted Polyoxometalates, *Fuel.*, **166**: 268-275 (2016).

[46] Trakarnpruk W., Jatupisarnpong J., Acidic and Cesium Salts of Polyoxometalates with and without Vanadium Supported on MCM-41 as Catalysts for Oxidation of Cyclohexane with H_2O_2, *Appl. Petrochem. Res.*, **3**: 9-15 (2013).

[47] Chamack M., Mahjoub A.R., Aghayan H., Cesium Salts of Tungsten-Substituted Molybdophosphoric Acid Immobilized onto Platelet Mesoporous Silica: Efficient Catalysts for Oxidative Desulfurization of Dibenzothiophene, *Chem. Eng. J.*, **255**: 686-694 (2014).

[48] Huixiong W., Mei Z., Yixin Q., Haixia L., Hengbo Y., Preparation and Characterization of Tungsten-substituted Molybdophosphoric Acids and Catalytic Cyclodehydration of 1,4-Butanediol to Tetrahydrofuran, *Chin. J. Chem. Eng.*, **17**: 200-206 (2009).

[49] Ding J., Zhiquan Y., Chong H., Xiaowen T., Ying L., Xiaojun N., Hongguo Z., UiO-66(Zr) Coupled with Bi_2MoO_6 as Photocatalyst for Visible-Light Promoted Dye Degradation, *J. Colloid Interface. Sci.*, **497**: 126-133 (2017).

[50] Yasmina T., Müller K., Synthesis and Characterization of Surface Modified SBA-15 Silica Materials and Their Application in Chromatography, *J. Chromatogr A.*, **1218**: 6464-6475 (2011).

[51] William H., Offeman R.E., Preparation of Graphitic Oxide, *J. Am. Chem. Soc.*, **80**: 1339-1339 (1958).

[52] Li W., Zhang B., Li X., Zhang H., Zhang Q., Preparation and Characterization of Novel Immobilized $Fe_3O_4@SiO_2@mSiO_2$–Pd(0) Catalyst with Large Pore-Size Mesoporous for Suzuki Coupling Reaction, *Appl. Catal. A.*, **459**: 65-72 (2013).

[53] Crake A., Christoforidis K.C., Kafizas A., Zafeiratos S., Petit C., CO_2 Capture and Photocatalytic Reduction Using bifunctional TiO_2/MOF Nanocomposites under UV–vis Irradiation, *Appl. Catal. B.*, **210**: 131-140 (2017).

[54] Fakhri H., Mahjoub A.R., Aghayan H., Effective Removal of Methylene Blue And Cerium by a Novel Pair Set of Heteropoly Acids Based Functionalized Graphene Oxide: Adsorption and Photocatalytic Study, *Chem. Eng. Res. Des.*, **120**: 303-315 (2017).

[55] Chamack M., Mahjoub A.R., Synthesis and Characterization of Supported $Cs_2H[PW_4Mo_8O_{40}]$ on Iron Oxide @ Mesoporous Silica Particles: Promising Catalyst for Oxidative Desulfurization Process, *Catal. Lett.*, **146**: 1050-1058 (2016).

[56] Chamack M., Mahjoub A.R., Aghayan H., Catalytic Performance of Vanadium-Substituted Molybdophosphoric Acid Supported on Zirconium Modified Mesoporous Silica in Oxidative Desulfurization, *Chem Eng Res Des.*, **94**: 565-572 (2015).

[57] Yang F., Li W., Tang B., Facile Synthesis of Amorphous UiO-66 (Zr-MOF) for Supercapacitor Application, *J. Alloys Compd.*, **733**: 8-14 (2018).

[58] Mardiroosi A., Mahjoub A.R., Fakhri H., Efficient Visible Light Photocatalytic Activity Based on Magnetic Graphene Oxide Decorated ZnO/NiO, *J. Mater Sci: Mater. Electron.*, **28**: 11722-11732 (2017).

[59] Torres-Garcia E., Galano A., Rodriguez-Gattorno G., Oxidative Desulfurization (ODS) of Organosulfur Compounds Catalyzed by Peroxo-Metallate Complexes of WOx–ZrO_2: Thermochemical, Structural, and Reactivity Indexes Analyses, *J. Catal.*, **282**: 201-208 (2011).

[60] Zhang Y., Wang R., Synthesis of silica@C-dots/phosphotungstates core-shell microsphere for effective oxidative-adsorptive desulfurization of dibenzothiophene with less oxidant, *Appl. Catal. B.*, **234**: 247- 259 (2018).

[61] Khodadadi A., Mokhtarani B., Mortaheb H.R., Deep and Fast Oxidative Desulfurization of Fuels Using Graphene Oxide-Based Phosphotungstic Acid Catalysts, *Fuel.*, **236**: 717-729 (2019).